

# Experimental Study of Natural Convective Flow over a Hot Horizontal Rhombus Cylinder Immersed in Water via PIV Technique

M. Karbasi pour, M. Nili-Ahmadabadi<sup>†</sup>, G. Taherian and A. Minaean

Department of Mechanical Engineering, Isfahan University of Technology, Isfahan, 8415683111, Iran

<sup>†</sup>Corresponding Author Email: [m.nili@cc.iut.ac.ir](mailto:m.nili@cc.iut.ac.ir)

(Received October 19, 2015; accepted December 22, 2016)

## ABSTRACT

Natural convective flow over a horizontal cylinder is a phenomenon used in many industries such as heat transfer from an electrical wire, heat exchanger, pipe heat transfer, etc. In this research, fluid dynamics of natural convective flow over a horizontal rhombus cylinder, with uniform heat flux, is investigated by using two-dimensional Particle Image Velocimetry (PIV) Technique. Experiments are carried out in a cubical tank full of water having an interface with air and the cylinder is placed horizontally inside the tank. The heater is turned on for 40s and the effects of heater's power and the height of water above the cylinder are surveyed. The experiments are carried out in three different heights of water and two different heater's powers in which Rayleigh number changes from  $1.33 \times 10^7$  to  $1.76 \times 10^7$ . The emitted heat flux causes the buoyancy force to be made and the main branch of flow to be formed. Then, moving up the main branch flow through the stationary water generates two equal anti-direction vortexes. These vortexes are developed when they reach the free surface. The results indicate that the flow pattern changes for different values of water height and heater's power.

**Keywords:** Natural convective; Rhombus cylinder; Heater; Velocity fields; PIV technique.

## NOMENCLATURE

$C_p$	specific heat capacity	$V_t$	total velocity
$d$	cylinder side	$V_{tmax}$	maximum total velocity
$g$	gravity acceleration	$x$	vertical position
$H$	height of water over the cylinder	$y$	horizontal position
$k$	conductivity		
$P$	heater's power	$\beta$	temperature expansion coefficient
$Ra$	Rayleigh number	$\nu$	viscosity
$t$	time	$\rho$	density
$t^*$	dimensionless time		

## 1. INTRODUCTION

In high-voltage power systems, passing electricity through wires causes its temperature to be increased and the wires to be damaged. Consequently, heat transfer enhancement of wires is very important for decreasing its temperature. Furthermore, heat transfer enhancement of pipes in heat exchangers has been conducted by many researches. To investigate this phenomenon, a lot of researches have been carried out experimentally, numerically, and analytically.

Study on natural convection was carried out

seriously by Nusselt (1920). Nusselt proposed Nusselt number as a non-dimensional number to state heat transfer rate from a solid surface to a fluid. Ackermann *et al.* (1932) experimentally measured heat transfer rate from a horizontal cylinder immersed in water to obtain the relation between the Nusselt and Rayleigh number.

Some of researchers investigated the fluid dynamics of natural convective flow.

Brodowicz (1966) obtained the distribution of temperature and velocity for the natural convective flow over a horizontal hot wire in air by PIV

technique. He observed a good agreement with other numerical investigations. Miyabe (1972) observed that natural convective flow of the plume above a hot horizontal cylinder starts to oscillate. In this regard, Morgan (1975) compared the experimental data of a large number of researchers and observed that there are many differences between them. He concluded that temperature measurement on the surface of cylinder had not been precise enough. Kitamura *et al.* (1999) investigated the natural convective flows of water around horizontal heated cylinders with diameters of 60-800 mm, experimentally. The main concerns of the mentioned study were the turbulent transition and its effect on the local heat transfer over a wide range of  $Ra_D$  from  $3.0 \times 10^8$  to  $3.6 \times 10^{13}$ . The results showed that three-dimensional flow separations occur first at the trailing edge of the cylinder when  $Ra_D$  is lower than  $2.1 \times 10^9$  and then, the separation points shift upstream with increasing the Rayleigh numbers. Ayani *et al.* (2005) numerically studied transient laminar natural convective flow over a line heat source in an unsteady state. The energy and momentum equations were solved for the fluid and solid (line heat source), simultaneously. Results indicated that the energy equation approaches to steady state more rapidly than the momentum equations. Grafsrñningen *et al.* (2011) experimentally investigated the characteristics of flow field above a uniformly heated horizontal cylinder in water. Mean and fluctuating velocity fields were presented for a range of Rayleigh numbers from  $2.05 \times 10^7$  to  $7.94 \times 10^7$ . Circumferential Nusselt number distributions were also presented. Velocity data was compared with existing similarity solutions of turbulent plumes. It was observed that the flow is initially laminar around the cylinder and then, undergoes a transition to turbulent flow at a distance above the cylinder. The point of starting the transition from laminar to turbulent flow travels upstream towards the cylinder with increasing Rayleigh number. Grafsrñningen *et al.* (2012) experimentally obtained temperature and velocity fields above an evenly heated horizontal cylinder with a Rayleigh number of  $9.4 \times 10^7$  using PIV and LIF technique, simultaneously. The vertical velocity and temperature field in the plume are compared with the similarity solutions of turbulent planar plumes. Kuehner (2012) investigated the fluid dynamics of natural convection around a heated horizontal cylinder using PIV technique. He carried out some experiments for  $Ra = 1.33 \times 10^6$  and different height ratios. Interaction of natural convective plume to the free surface was observed for all height ratios. He observed that free surface doesn't impose oscillatory motion for the height ratio of  $H/D = 2$  and  $H/D = 8$ . Based on the research, a vortex along the fluid plume rising up towards the free surface separates from the plume and shifts its direction to the free surface. They also investigated the effect of plume swaying and plume formation. Measurements showed that convection in plume flow makes some differences in boundary layer. The effect of these differences diffuses from downstream into the plume formation region

(2015).

Understanding flow characteristics is necessary and important in order to evaluate its effects on heat transfer. For example Koizumi (1996) examined the impact of ceiling on the performance of flow and heat transfer around a horizontal cylinder. Atmane (2003) studied the effect of vertical confinement on the natural convection flow and heat transfer around a horizontal heated cylinder by PIV technique. The flow characteristics and the time-resolved heat transfer were measured respectively above and around the cylinder. It was shown that the primary effect of the vertical confinement is an increase in heat flux on the upper part of the cylinder for given separation distances between the cylinder and the fluid boundary. This increase was shown to be related to the large-scale oscillation of the thermal plume.

Beside these investigations, industrial applications led researcher to study the free convection flow around non-circular cylinders.

Nakamura and Asako (1978) investigated the free convection flow of a horizontal cylinder with arbitrary shape by constant heat flux and temperature boundary conditions. In experiments they measured average heat transfer coefficient 10 to 30 percent more than calculated values earned from theoretical investigation. Cheng (2006) studied the free convection flow and heat transfer of micropolar fluids around an elliptic cylinder numerically. He found that heat and mass transfer from an elliptic cylinder in vertical position is more than horizontal. Ahmad *et al.* (2008) studied the boundary layer flow of free convection flow over an elliptic cylinder with constant heat flux and found that temperature and velocity distributions, friction coefficient and cylinder surface temperature will be reduced with increasing Prandtl number. Sakr *et al.* (2008) conducted some experiments and numerical analysis on similar problem with an elliptic cylinder inside a circular channel. They concluded that an increase in Rayleigh number and decrease in hydraulic diameter increases Nusselt number. Kumar-De and Dalal (2006) studied natural convection from a hot titled square in an enclosure with cold walls numerically. They analyzed the effect of the type of boundary condition, aspect ratio of the cylinder and location of the cylinder in enclosure on flow and heat transfer parameters. The application of this investigation is in electronic modules that are encapsulated inside a chamber. In these cases the effect of the cooling is dependent to the wall effect.

In this study the behavior of free convection flow of water around a rhombic cylinder is investigated experimentally. The fluid flow is visualized with Particle Image Velocimetry (PIV) technique. The effects of the water height above the cylinder and heat flux on the plume characteristics are studied. Furthermore, velocity profiles at each time are obtained and the movements of vortexes beside the plume are investigated.

## 2. EXPERIMENTAL FACILITY AND METHOD

In the experimental test bed, a cubic tank, which its walls are made of Plexiglas, is used as shown in Fig. 1. A rhombus cylinder with constant heat flux is used for heat generation in the water tank. The generated heat can be varied from 0 to 200W by a dimmer. Each side of the rhombus is 1cm long and the angle between its sides is 90 degrees. The dimmer adjusts the inputted voltage into the heater to control the rate of heat flux. The cylinder is placed at a distance of 7.5 cm from the bottom of the tank and on the symmetric line of the tank. Hollow Glass Spheres with the size of 10 and 20 $\mu$ m, and the density of 1.35 kg/m<sup>3</sup> are poured into the water to move along the flow streamlines and to show flow direction and velocity components in each point. A laser beam is emitted from a 200mW-DPSS continuous laser. The emitted beam is converted to a laser sheet by a cylindrical lens. The green laser sheet lights a plane of fluid through which the particles movement can be seen. The particles are so sensitive to the laser light that can be tracked by a camera. Here, a CCD camera with a resolution of 600 $\times$ 800 pixel<sup>2</sup> and capture rate of 25 frames per second takes many sequential photos to monitor the particles, moving through the lighted sheet. To measure velocity field in an instant, the two sequential photos are analyzed by image processing. This process and analysis is carried out for the consecutive instants of a time range to obtain time-dependent flow field. Considering the capture rate of camera, 24 velocity fields can be obtained through each second.

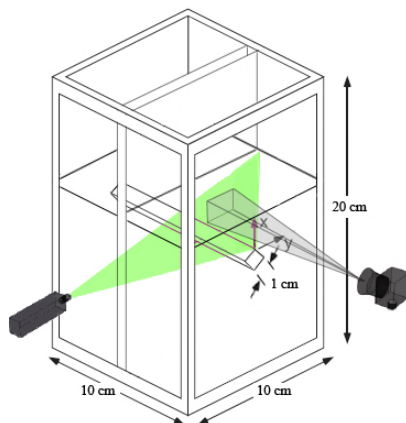


**Fig. 1. Experiment test bed and coordinate system reference.**

The experiments are carried out in six different states with the H/d of 4, 7 and 11, and the heater's powers of 100 and 200W. The change of heat flux is described by Rayleigh number:

$$Ra = \frac{g\beta q'' \rho_0 C_p d^4}{k^2 \nu} \quad (1)$$

where  $g$  is gravity acceleration,  $\beta$  is temperature expansion coefficient,  $\rho$  is fluid density,  $C_p$  is

specific heat capacity,  $d$  is the cylinder side,  $k$  is the fluid conductivity and  $\nu$  is the fluid viscosity. Also non-dimensional time is represented by:

$$t^* = \frac{t V_{tmax}}{d} \quad (2)$$

where  $t$  is time,  $V_{tmax}$  is the maximum value of total velocity and  $d$  is the cylinder side.

As shown in Fig. 1, the reference coordinate is placed on the center of rhombus cylinder. Some symbols are introduced in Table 1 to simplify the naming of analysis results.

**Table 1 Experiment states**

states	x/d	Power of heater (W)	Ra
A <sub>1</sub>	4	100	5.9 $\times$ 10 <sup>6</sup>
A <sub>2</sub>	4	200	1.2 $\times$ 10 <sup>7</sup>
B <sub>1</sub>	7	100	5.9 $\times$ 10 <sup>6</sup>
B <sub>2</sub>	7	200	1.2 $\times$ 10 <sup>7</sup>
C <sub>1</sub>	11	100	5.9 $\times$ 10 <sup>6</sup>
C <sub>2</sub>	11	200	1.2 $\times$ 10 <sup>7</sup>

According to measurements, the maximum total velocity for  $Ra = 5.9 \times 10^6$  is 16 mm/s and for  $Ra = 1.2 \times 10^7$  is 28.9 mm/s. The non-dimensional time is defined based on these maximum velocities.

## 3. RESULTS AND DISCUSSION

### 3.1 A<sub>1</sub> State

Here, the effect of height of water (H/d) and Rayleigh number on the flow field are studied. Therefore, the fluid flow is analyzed from the moment that the heater has been turned on for  $\Delta t^* = 64$ . This range of time is enough to capture all states of flow behavior in this study. After  $t^* = 64$ , the flow behaviors are just repeated periodically. Moreover, there is a good repeatability between the similar tests. Once the heater is turned on, heat starts to be emitted to its surrounding water. It causes the water to be warmed and its density to be decreased. Consequently, buoyancy force is strengthened and rises up the fluid from the cylinder surrounding. It represents the start of plume formation named as "main branch flow". As seen in Fig. 2, due to the buoyancy force, the heated fluid particles rises up toward the free surface and another ones with a lower temperature is substituted, continuously. Moreover, the main natural convective flow is created along the sides of the rhombus.

Exact monitoring of the flow field in this state indicates that the flow behavior can be divided in three phases. In the first phase, once the heater is turned on, a plume around the heater is formed. Then, it moves toward the free surface under the influence of buoyancy force and forms the main branch flow (Fig. 3). The plume moving toward the

free surface creates velocity gradients between the main branch flow and its surrounded stationary fluid. Therefore, two vortices are generated from the both sides of the main branch. Considering that circulation around the cylinder is zero when the fluid is stationary at  $t^* = 0$ , the two vortices should neutralize each other immediately after turning on the heater. As shown in Fig. 3, in  $A_1$  state, these two vortices are almost symmetric at the initial moments of the plume formation.

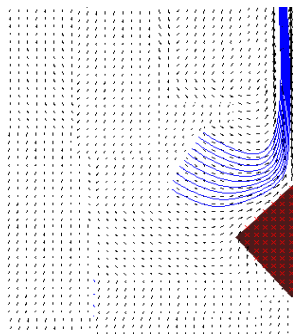


Fig. 2. Streamline of velocity field around cylinder.

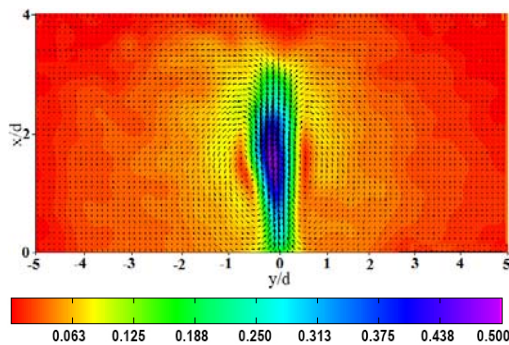


Fig. 3. Velocity field at  $Ra = 5.9 \times 10^6$  ( $A_1$  state),  $t^* = 3.2$  after turning on the heater.

In the second phase, the main branch flow interacts with the free surface and changes into two sub-branches with deflecting  $90^\circ$  respect to its direction. Afterward, the two vortices are intensified and then stretched under the sub-branches so that the two sub-branches reach the two upper corners of the tank. Here, the angle between the main branch and the two sub-branches are approximately equal to  $90^\circ$ . As seen in Fig. 4, the initial formed vortices rise up with the plume towards the free surface and then, direct the sub-branches flow toward the two upper corners parallel to the free surface. Over time, the sub-branches return down and join to the main branch flow. Then, the formed vortices under the sub-branches become smaller. As shown in Fig. 5, because the vortices become smaller, the sub-branches flow are inclined to the main branch flow, thus the angle between the main and sub-branches reduces from  $90^\circ$  to  $45^\circ$ .

In the third phase, intersection of the returned flow with the main branch makes it to oscillate with the period of  $\Delta t^* = 5.76$ . The computed period is the

time through which the main branch returns to the primitive position. In this movement, the main branch flow oscillates towards the left and right with a large amplitude. The contours of velocity vectors for the period of an oscillation are indicated in Fig. 6. In this period, the main branch moves from one side to another and then, returns again to its initial location. In Fig. 6, each contour indicates the flow field through its mentioned time interval. Deviation of the main branch flow to one side causes the returned flow of the sub branch at the same side to be strengthened and consequently, it will interact with the main branch flow, more strongly. This phenomena eventuates deviation of the main branch to the opposite side.

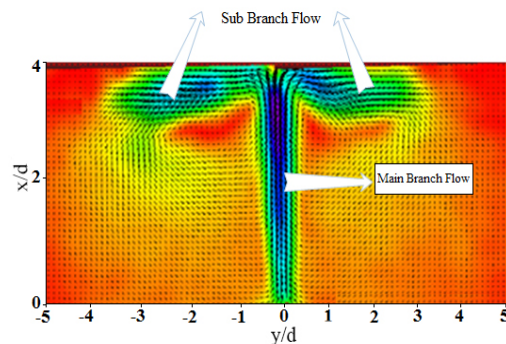


Fig. 4. Velocity field at  $Ra = 5.9 \times 10^6$  ( $A_1$  state),  $\Delta t^* = 9.6$  after turning on the heater.

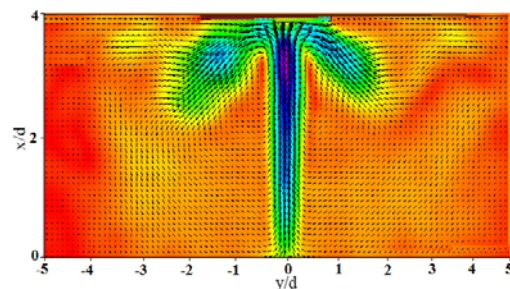


Fig. 5. Velocity field at  $Ra = 5.9 \times 10^6$  ( $A_1$  state),  $\Delta t^* = 19.2$  after turning on the heater.

### 3.2 $A_2$ State

In  $A_2$  state, increasing Rayleigh number by increasing the heater's power intensifies the buoyancy force. It causes the main branch is formed more quickly than  $A_1$  state and the sub-branches spread to the upper corners of the tank with more momentum. As shown in Fig. 7,  $L_2$  representing the spread length of the sub-branch in  $A_2$  state is greater than  $L_1$  related to  $A_1$  state. In this state unlike  $A_1$  state, there is no oscillation with large amplitude and period. Investigation of the third phase of motion in  $A_1$  state indicates that the time interval between formation and destruction of the sub-branches vortices is large. Thus, the period and amplitude of the oscillations is large and its flow field is regular. In  $A_2$  state, because of large velocity magnitude, the returned flow from the sub-branches interacts with the main branch more

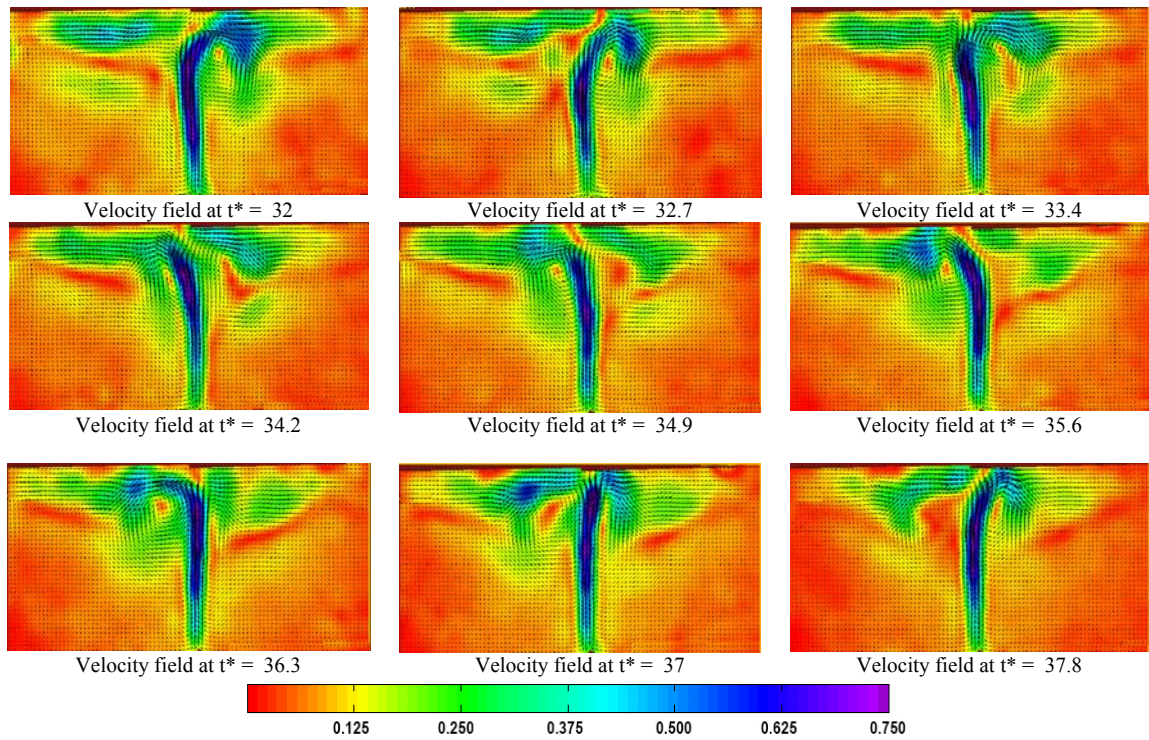


Fig. 6. Velocity field at  $Ra = 5.9 \times 10^6$  ( $A_1$  state) in the range of  $t^* = 32$  to 37.8.

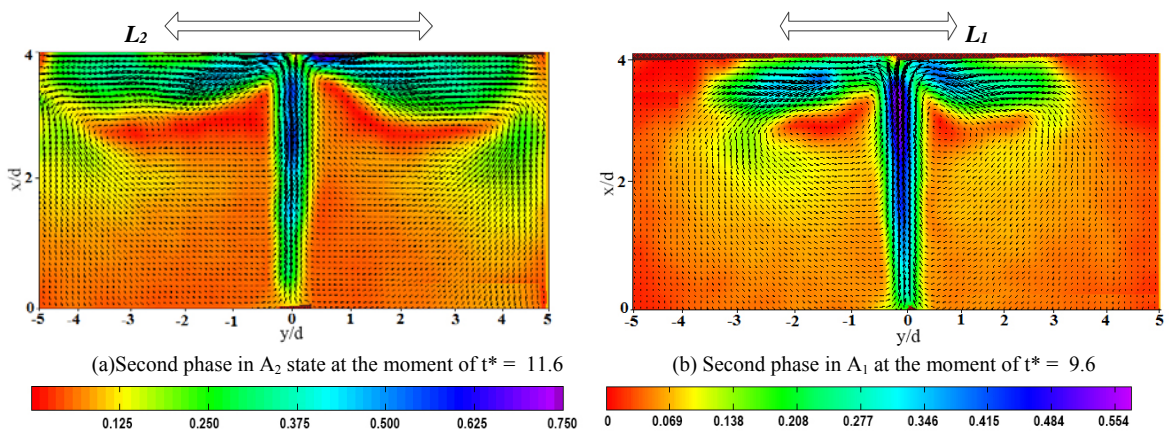


Fig. 7. Comparison of spread length of sub-branches in  $Ra = 5.9 \times 10^6$  ( $A_1$  state) and  $Ra = 1.2 \times 10^7$  ( $A_2$  state).

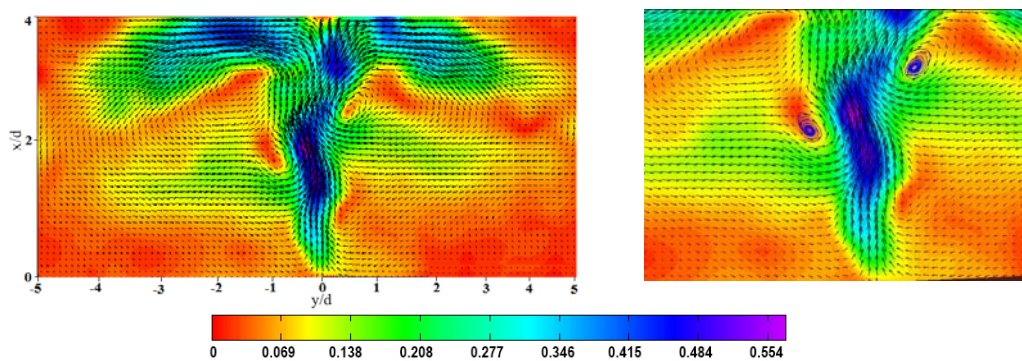


Fig. 8. Velocity field at third phase of motion,  $Ra = 1.2 \times 10^7$  ( $A_2$  state) and moment of  $t^* = 72.3$ .

strongly as shown in Fig. 8. It locally intersects the main branch and makes it to be non-uniform and wavy; thus, the oscillations of the main branch have

a higher frequency. In other words, increasing the Rayleigh number intensifies the vortices and increases the frequency of oscillations.

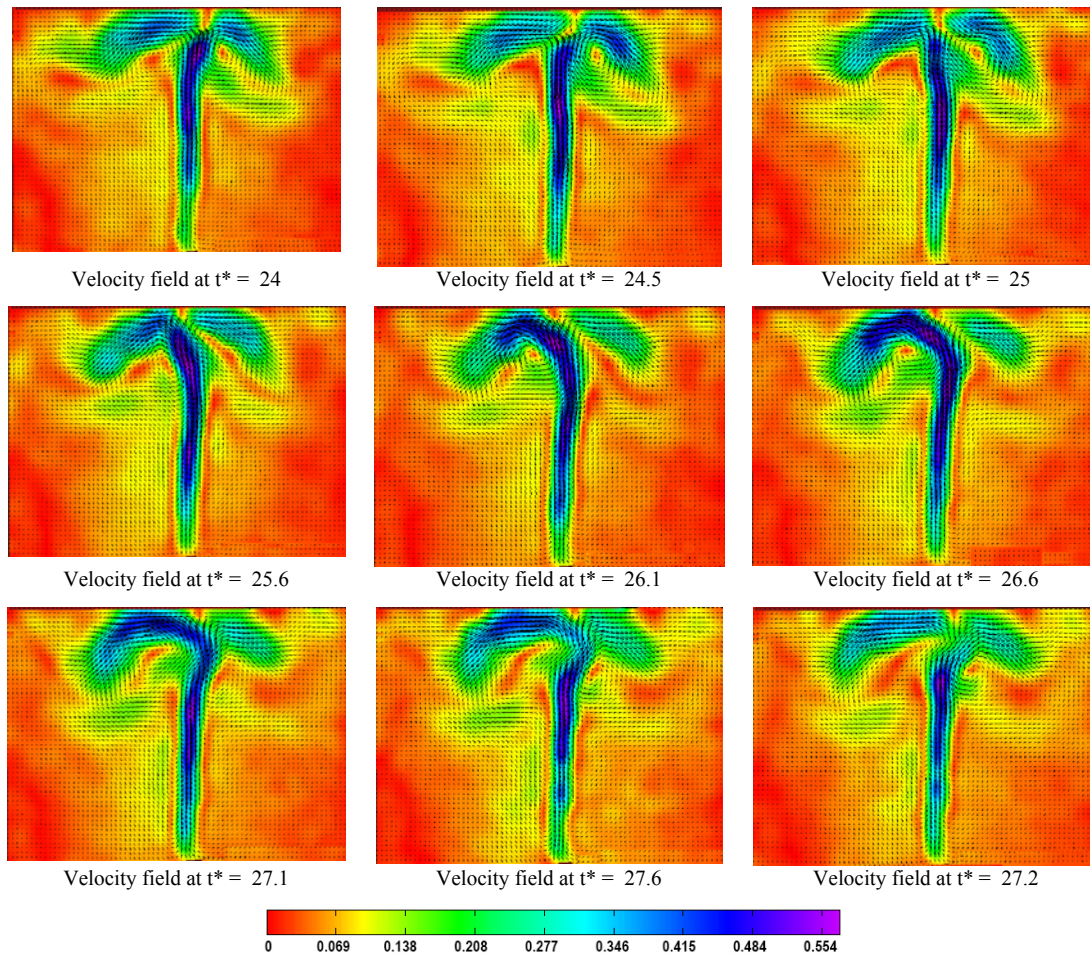


Fig. 9. Velocity field at  $Ra = 5.9 \times 10^6$  ( $B_1$  state) in the range of  $t^* = 28.2$  to  $50.9$ .

### 3.3 $B_1$ State

In this state, due to increase of  $H/d$ , the flow momentum can't cope with the weight of water height, and the main branch flow reaches the free surface with less momentum. As a result, the main branch through its end quarter becomes unstable sooner than that in  $A_1$  state. The flow pattern of  $B_1$  state is similar to  $A_1$  state except that the flow is more unstable and the oscillation period of the main branch reduces from  $t^* = 5.8$  to  $t^* = 4.2$ . In other words, flow instability depends on two main characteristics; flow velocity, and water height above the cylinder or length characteristic. In  $B_1$  state, increase of the height leads to instability. The unsteady flow field of  $B_1$  state is shown in Fig. 9.

### 3.4 $B_2$ State

In  $B_2$  state, due to increase of the Rayleigh number, the instability increases and it causes the main branch to be wavy. In this state, two vortexes are asymmetrically shed from the second half of the main branch and rise up toward the free surface. Vortex shedding of  $B_2$  state is shown in Fig. 10.

### 3.5 $C_1$ State

In this state, the Rayleigh number is low and the  $H/d$  is large; then, the flow momentum can't cope

with the weight of water height and the plume becomes unstable. As shown in Fig. 11 against  $A_1$  state, the plume moves towards the free surface, asymmetrically.

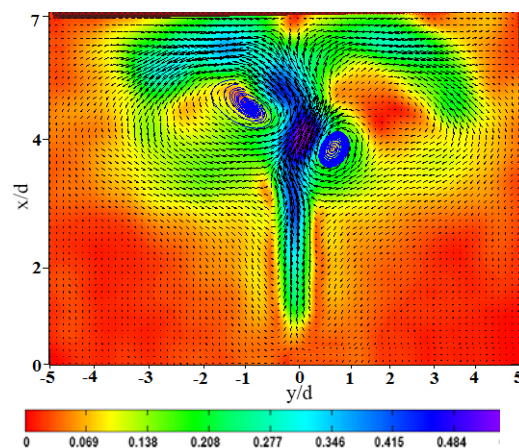


Fig. 10.  $Ra = 1.2 \times 10^7$  ( $B_2$  state) at the moment of  $t^* = 43.4$ .

Through the third phase of its motion, the returned flow of the sub-branches interact the main branch

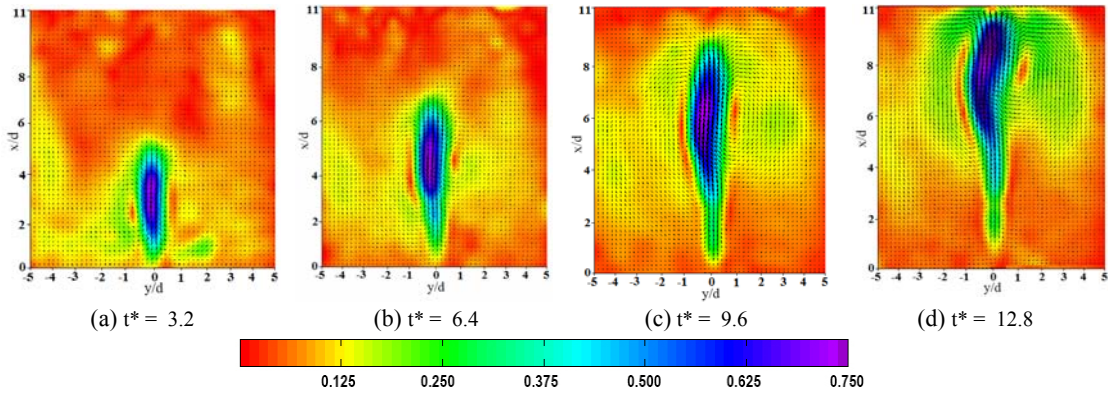


Fig. 11. Velocity field of the first phase of motion, at  $Ra = 5.9 \times 10^6$  ( $C_1$  state).

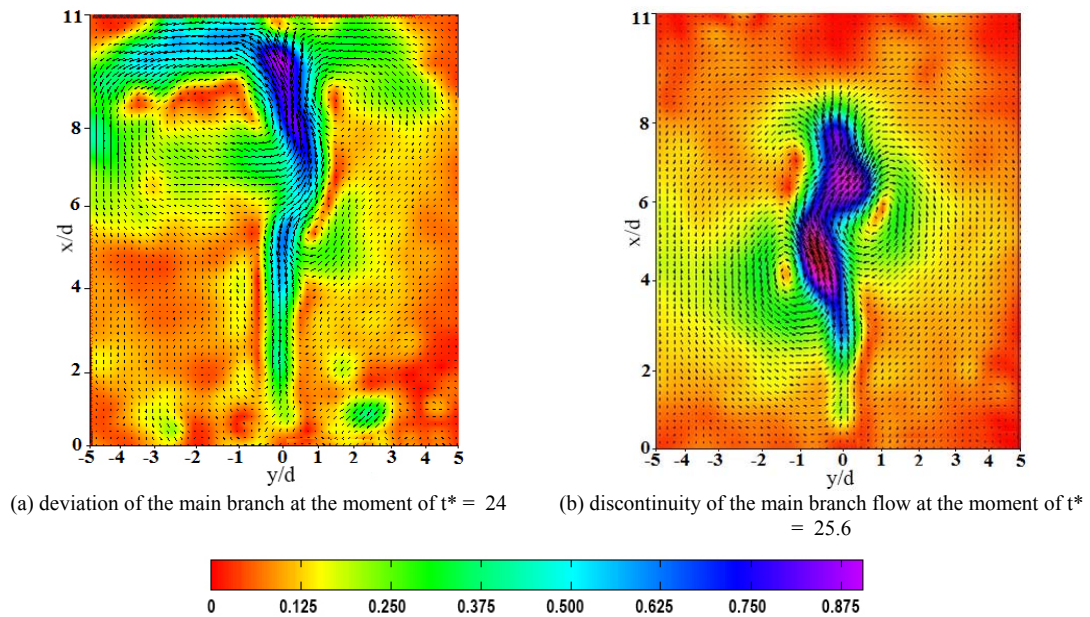


Fig. 12. The velocity field at  $Ra = 5.9 \times 10^6$  ( $C_1$  state).

and it leads to discontinuity of the main branch. As shown in Fig. 12, because of low momentum of the main branch, the returned flows intersect the main branch and causes separation of the main branch.

### 3.6 $C_2$ State

Increasing the Rayleigh number in  $C_2$  state causes the rising plume to be more unstable and asymmetric than that in  $C_1$  state (Fig. 13). It is because of the larger velocity magnitude and water height.

In Fig. 14, oscillations of the main branch at the third phase and related vortices have been shown. Comparison between this figure and Fig. 8, related to  $A_1$  state, indicates that the number of created vortices have been increased in  $C_2$  state. Furthermore, because of more instability in  $C_2$  state, the amplitude and frequency of the oscillation along the main branch have been increased.

At the third phase of motion, because of increasing the Rayleigh number, the buoyancy force and the

main branch momentum increase. Thus, interaction between the returned flow and main branch can't cause separation in the main branch. The third phases of motion in  $C_1$  and  $C_2$  states have been compared in Fig. 15. As seen, there is no separation in  $C_2$  state unlike  $C_1$  state. Over time, the interaction between the main branch and sub-branches is intensified which causes the oscillations amplitude to be increased.

### 3.7 Temporal Behavior of Velocity in Symmetric Line

Here, the temporal behavior of velocity magnitude along the symmetric line is studied at the three points of  $(x/4d)$ ,  $(x/2d)$  and  $(3x/4d)$  above the cylinder when the heater is turned on. As shown in Fig. 16, velocity distributions versus time are plotted for  $A_1$ ,  $B_1$  and  $C_1$  states. In other words, the effects of changing the free surface height on the velocity changes and fluctuations are investigated. According to this figure, in  $A_1$  state, the fluctuations at  $x/2d$  are more than the others. By increasing the

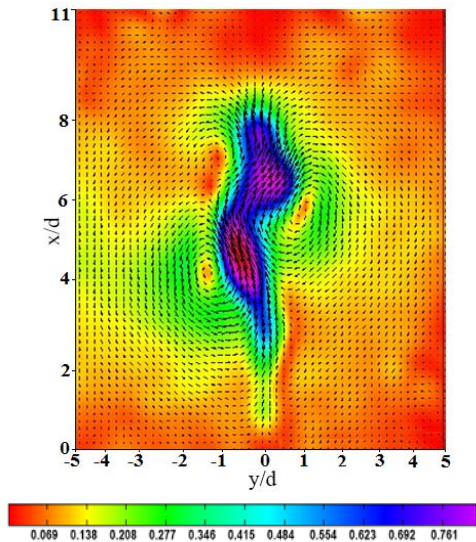


Fig. 13. First phase of motion in  $C_2$  state, at the moment of  $t^* = 8.7$ .

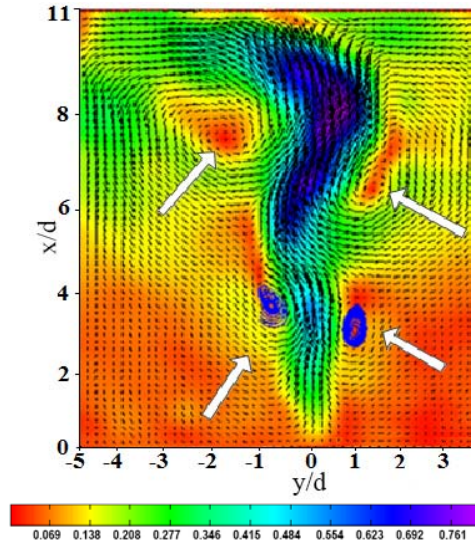
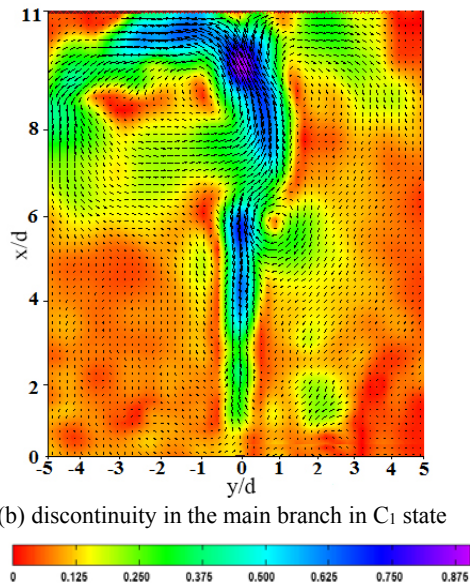
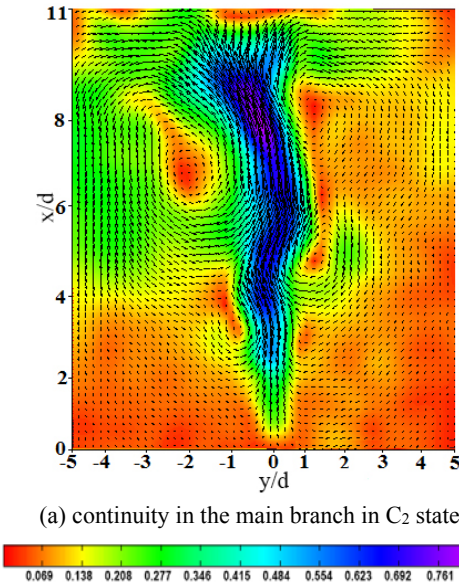


Fig. 14. Third phase of motion in  $C_2$  state, at the moment of  $t^* = 57.8$ .



(b) discontinuity in the main branch in  $C_1$  state



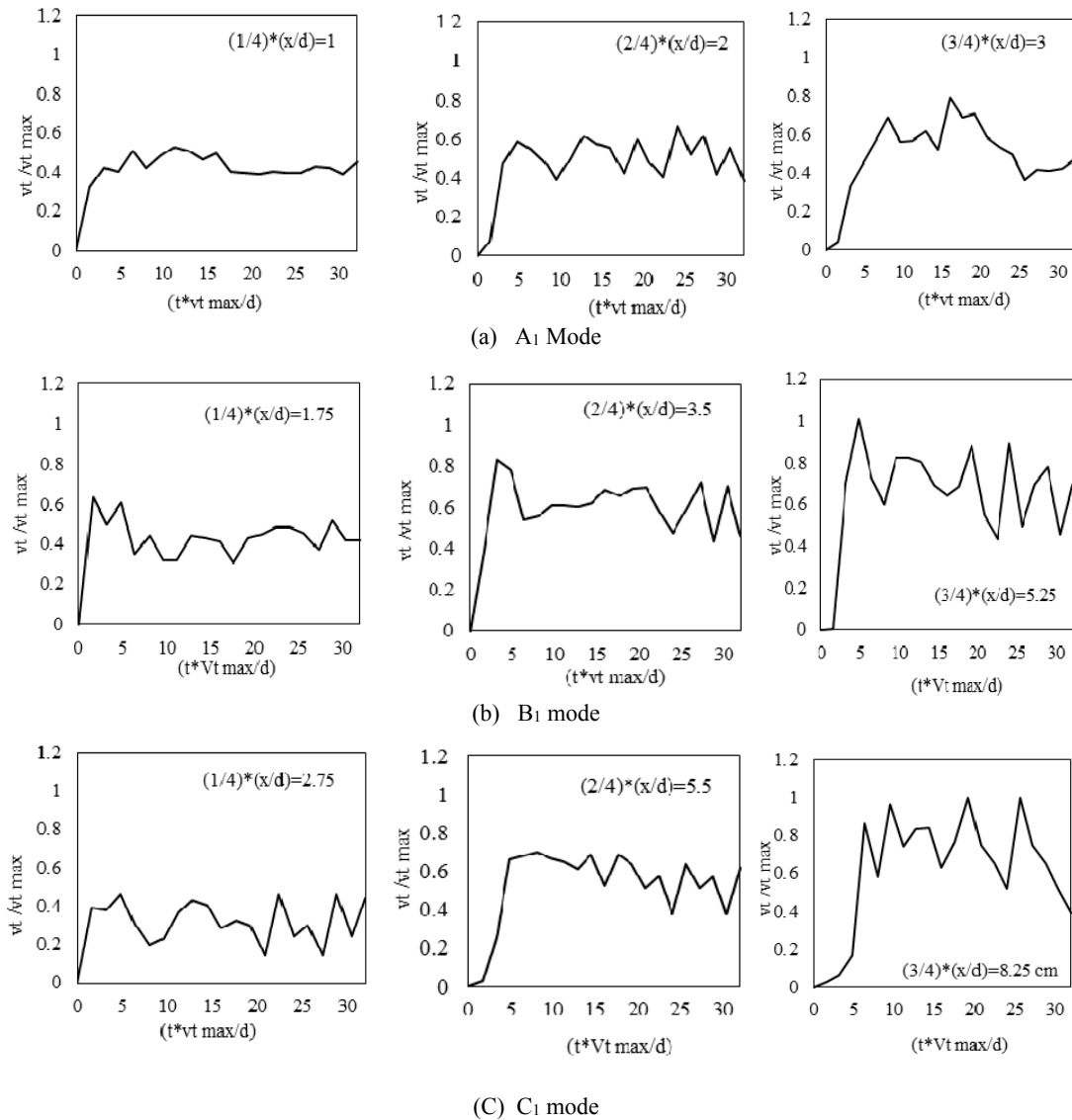
(a) continuity in the main branch in  $C_2$  state

Fig. 15. Comparison between the velocity fields of the third phase of motion related to  $C_1$  and  $C_2$  state at the moment of  $t^* = 25.6$  and  $46.2$ , respectively.

$H/d$  in  $B_1$  and  $C_1$  states, the fluctuations near the free surface at  $3x/4d$  increase. Also, as expected, the minimum fluctuations occur at the lower layers of fluid at  $x/4d$ . Moreover, in each three states of  $A_1$ ,  $B_1$  and  $C_1$ , the mean velocity increases when fluid particles move from  $x/4d$  to  $3x/4d$ . It indicates that the buoyancy force accelerates the fluid particles along the symmetric line. It is worth noting that increasing  $H/d$  from  $A_1$  to  $B_1$  mode increases the mean velocity while from  $B_1$  to  $C_1$  mode, it decreases the mean velocity so that the maximum mean velocity occurs in  $B_1$  mode. It shows that the buoyancy force generated from the cylinder with  $Ra = 5.9 \times 10^6$  cannot efficiently accelerate the water column with  $H/D = 11$  in  $C_1$  mode. Also, in  $A_1$  mode, due to less height, there is not enough time

for the buoyancy to accelerate the water column. Therefore, there is an optimum ratio of water height to heater's power in which the mean velocity and heat transfer reaches to its maximum. Here, the results show that this optimum ratio is about  $0.07 \text{ cm/W}$ .

In Fig. 17, when the Rayleigh number increases, the velocity fluctuations and mean velocity increase compared to Fig. 16. In  $A_2$  mode, due to low ratio of water height to heater's power, the water above the cylinder is accelerated very fast and the mean velocity reaches its maximum at the point of  $x/2d = 2$ . Afterward, the water particles are decelerated through a distance of  $x/2d = 2$  from  $x/2d$  to the free surface so that the mean velocity has been



**Fig. 16. Time history of velocity magnitude along the symmetric line for A<sub>1</sub>, B<sub>1</sub>, C<sub>1</sub> modes.**

decreased at  $3x/4d = 3$ . In B<sub>2</sub> mode, the mean velocity at  $x/2d$  and  $3x/4d$  is almost equal and the water particles are decelerated after the point of  $3x/4d = 5.25$ . In C<sub>2</sub> mode, there is almost the same behavior observed in B<sub>2</sub> mode. It is worth noting that unlike Fig. 16, increasing the  $H/d$  from 4 to 11 increases the mean velocity so that the maximum mean velocity occurs in C<sub>2</sub> mode. Here, the maximum ratio of water height to heater's power reaches 0.055 cm/W that is less than the optimum ratio of 0.07 cm/W.

### 3.8 Velocity Profile Through the Time of Plume Formation

In this section, the vertical and horizontal velocity profiles at the time of plume formation are studied. The results indicate that the velocity profiles through the three regions showed in Fig. 18 are different due to the formation of two vortices at the

time of the plume rising up.

At the top of the plume which is called A region, the horizontal velocity is negative on its left and positive on its right. Also, the vertical velocity is positive through the A region.

Through the region of the vortex formation, which is called B region, the horizontal velocity is low and the vertical velocity is positive near the symmetric line and negative through the lateral layers. Moreover, in B region, the horizontal velocity is positive on the right and negative on the left. The behavior of the horizontal velocity through the C region is unlike the A region. It means that it is positive on its left and negative on its right.

To study the behavior of the plume at different modes, the horizontal and vertical velocity profiles of the plume at different sections are obtained at  $t = 1s$  and  $t = 2s$ .

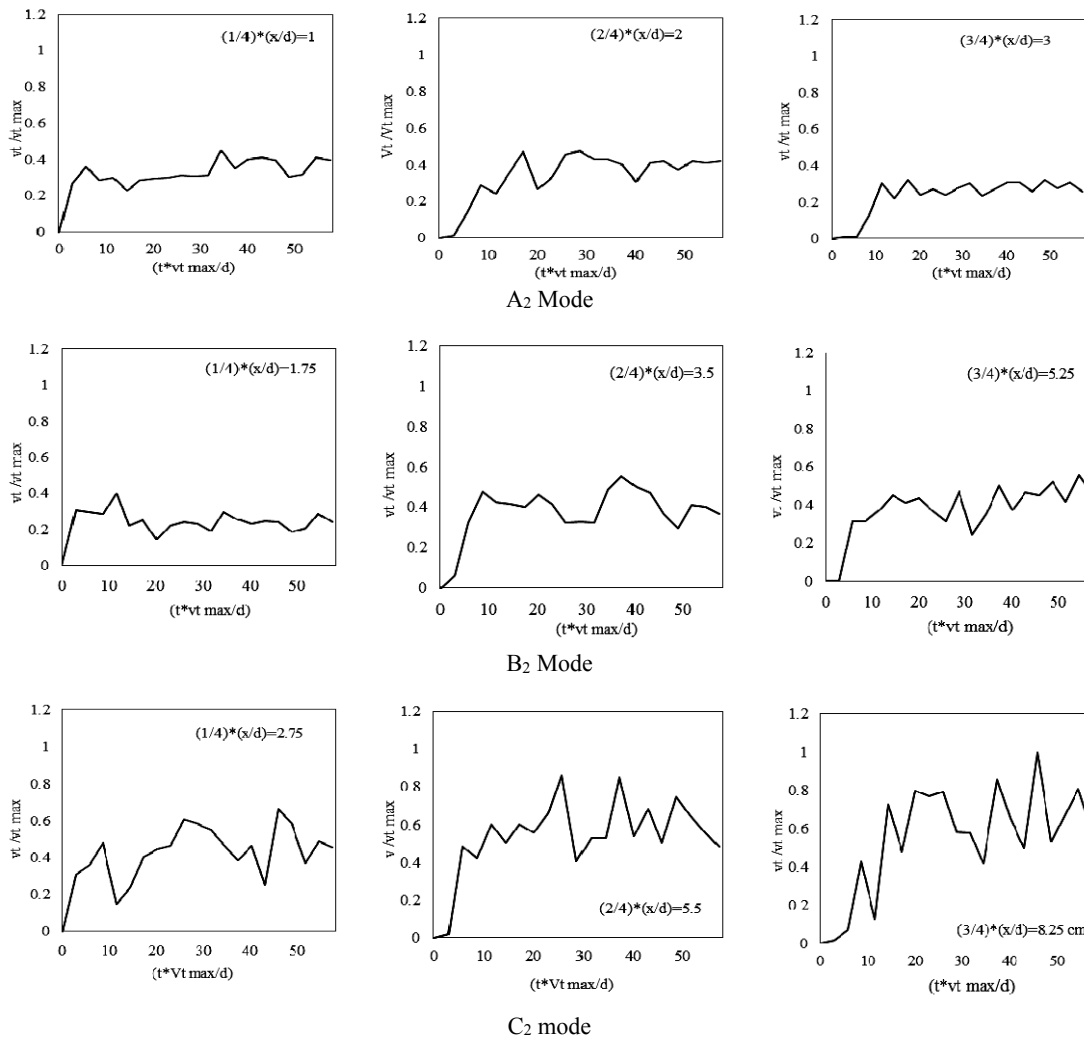


**Fig. 17.** Time history of velocity magnitude along the symmetric line for  $A_2$ ,  $B_2$ ,  $C_2$  modes.

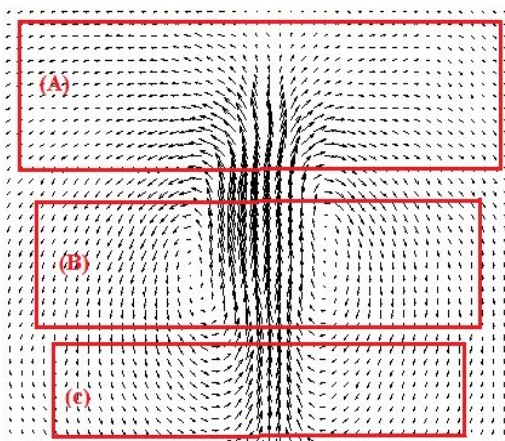


**Fig. 18.** Different regions of raising plume.

As shown in Fig. 19, the horizontal and vertical velocity profiles are plotted on the sections of  $x/d = 1$  and  $x/d = 2$  above the cylinder at  $A_1$  mode. It is noticeable that the effects of the free surface on the velocity profiles at of  $x/d = 1$  and  $x/d = 2$  are negligible. At  $t^* = 1.6$ , through both sections of  $x/d$

$= 1$  and  $x/d = 2$ , the horizontal velocity is negative on the left and positive on the right that relates to the B region. At  $t^* = 3.2$  and  $x/d = 1$ , the horizontal velocity becomes positive on the left and negative on the right that is vice versa compared to that on  $x/d = 2$ . It shows that the formed vortices have risen up so that  $x/d = 1$  is inside the C region but,  $x/d = 2$  is still inside the B region. Furthermore, the symmetry of the horizontal velocity at  $t^* = 1.6$  has been destroyed at  $t^* = 3.2$ . At  $t^* = 1.6$ , the vertical velocity on  $x/d = 1$  outside the plume region is more negative than that on  $x/d = 2$  while on  $x/d = 1$  inside the plume region, it is more positive than that on  $x/d = 2$ . It shows that at  $t^* = 1.6$ ,  $x/d = 1$  is in the middle of the B region while  $x/d = 2$  is at the top of the B region. At  $t^* = 3.2$ , it is exactly vice versa that indicates  $x/d = 2$  is in the middle of the B region. Therefore, it can be concluded that the maximum velocity occurs in the middle of B region that is related to  $x/d = 1$  for  $t^* = 1.6$  and  $x/d = 2$  for  $t^* = 3.2$ . Moreover, the maximum velocity increases versus time due to the plume acceleration resulted from buoyancy force. An almost similar behavior can be seen for  $A_2$ ,  $B_1$  and  $B_2$  modes.

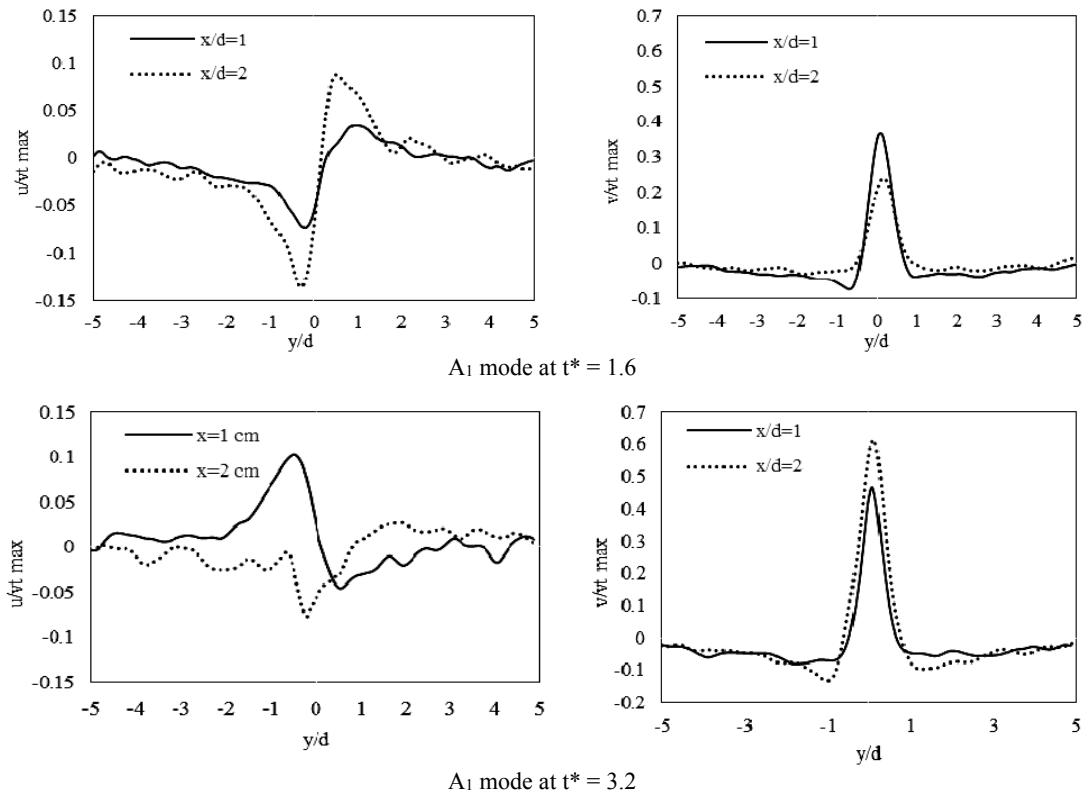


**Fig. 19. Horizontal and vertical velocity profiles at  $A_1$  mode.**

In Fig. 20, the velocity profiles are plotted for  $C_1$  mode along the three sections of  $x/d = 2, 3$  and  $4$ . At  $t^* = 1.6$ , the horizontal velocity on  $x/d = 2$  is positive on the left and negative on the right, and on  $x/d = 3$  and  $4$ , it is vice versa. At  $t^* = 1.6$ , the maximum velocity occurs through  $x/d = 3$  indicating that this section is in the middle of B region. At  $t^* = 3.2$ , the horizontal and vertical velocity profiles show that  $x/d = 4$  is in the middle of B region. Moreover, the horizontal velocity profiles in  $C_1$  mode are asymmetric indicating the plume instability and asymmetrical growth of the vortices when the  $H/d$  increases.

In Fig. 21, the velocity profiles are plotted for  $C_2$  mode. As seen, the vertical and horizontal are asymmetric especially at  $t^* = 5.8$ . It indicates that increasing the  $H/d$  and  $Ra$  increases the plume instability.

#### 4. CONCLUSION

In this research, free convective flow over a hot horizontal rhombus cylinder immersed in water was experimentally studied by PIV technique. Based on this research, three phases of motion were observed for flow around the heater; 1- forming a warmed plume rising up toward the free surface (main branch) 2- interaction of the main branch with the free surface and forming two sub-branches 3- forming returned flow from sub-branches and intersecting the main branch.

It was observed that in both  $A_1$  and  $B_1$  states, the main branch oscillates with respectively  $\Delta t^* = 5.8$  and  $4.2$  periods. In  $B_1$  state, the oscillation period was increased because of increasing the water height ( $H/d$ ) as a characteristic length.

In  $A_2$  state, by increasing the Rayleigh number and buoyancy force, the momentum of sub-branches was increased and thus, the returned flows had more momentum. Therefore, an intensive interaction between the returned flow and the main branch was occurred. It caused the main branch to be obstructed and its velocity to be non-uniform. This intensified oscillatory motions and flow instability. This phenomenon was intensified by increasing  $H/d$  ( $C_1$  and  $C_2$  states).

Study of velocity magnitude along the symmetric line versus time showed that there is an optimum ratio of  $H/d$  to the  $Ra$  in which flow velocity and heat transfer can reach its maximum value. For ratios less than this optimum value, there is not enough time for buoyancy to accelerate the fluid particles above the cylinder. Also for ratios more than the optimum value, the buoyancy cannot overcome the  $H/d$  so efficiently that the main branch is interrupted through the middle of path.

Furthermore, the vertical and horizontal velocity profile of the plume at the time of forming showed that the plume has three different regions that the maximum velocity occurs through the middle region called B region.

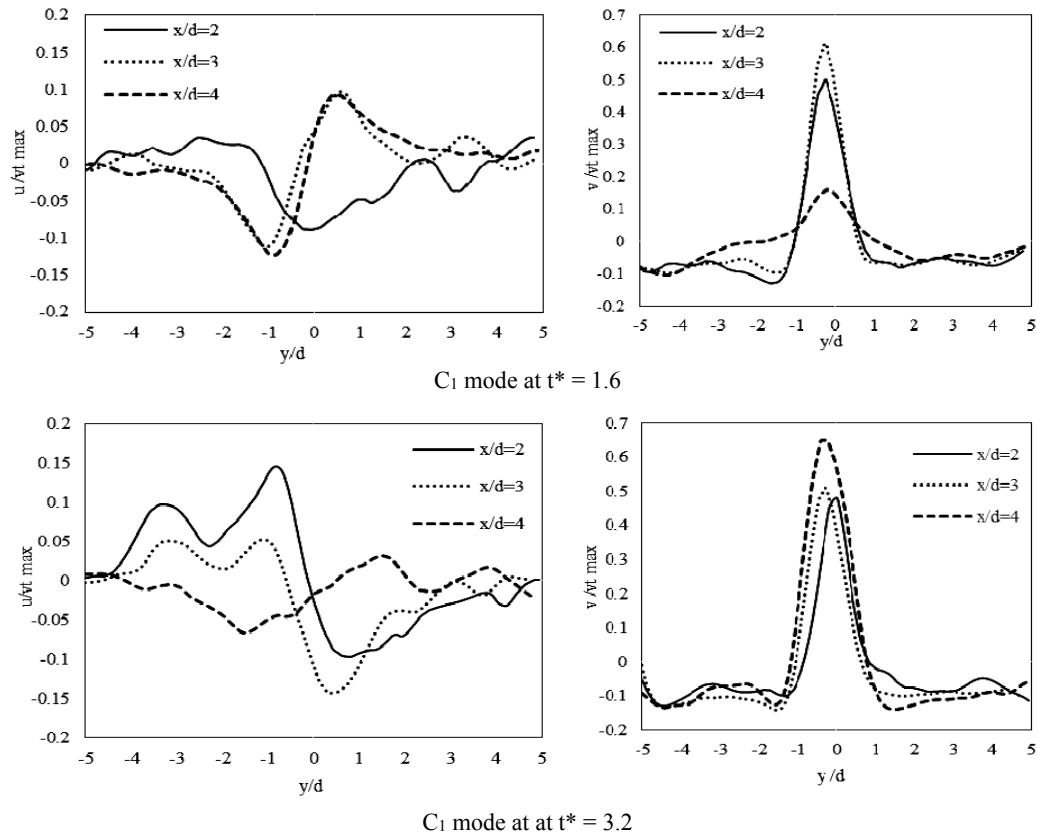


**Fig. 20. Horizontal and vertical velocity profiles at  $C_1$  mode.**

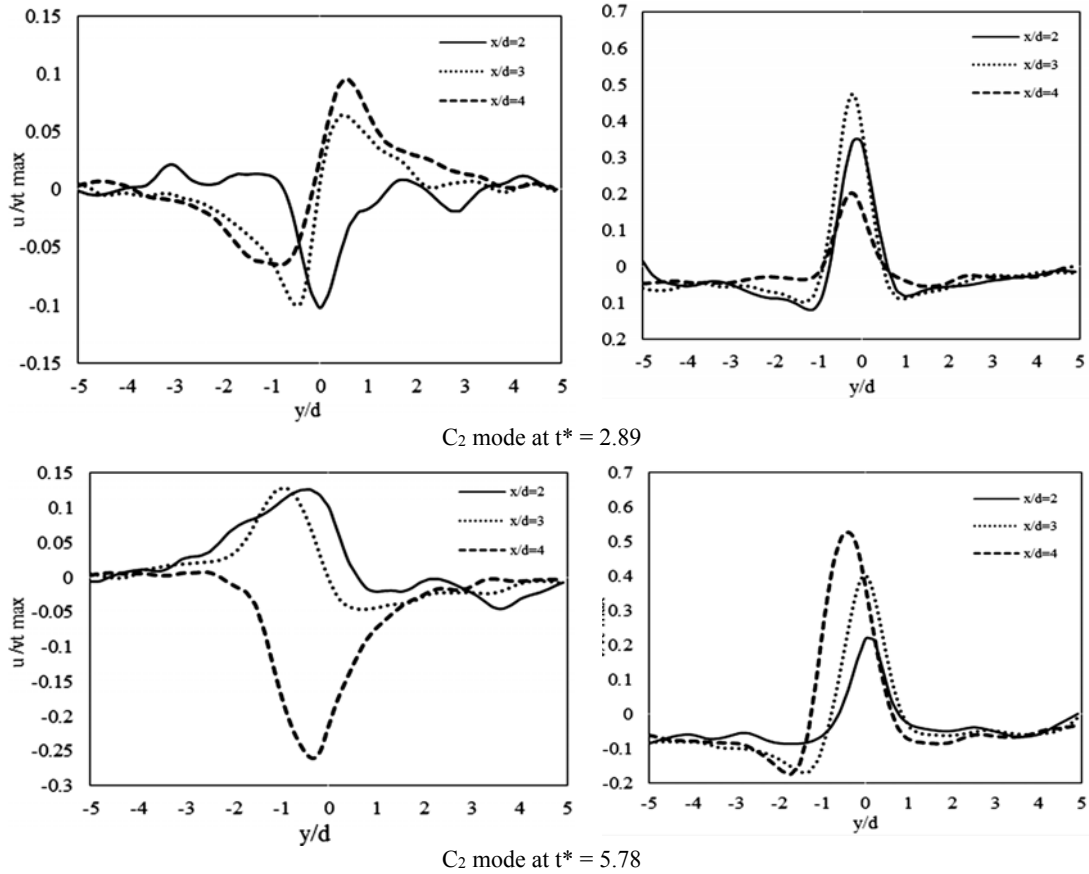


**Fig. 21. Horizontal and vertical velocity profiles at  $C_2$  mode.**

## REFERENCES

- Ackermann, G. (1932). Die Wrmeabgabe eines horizontalen geheizten Rohres a kaltes Wasser bei natrlicher Konvektion, *Forsch. Geb. Ingenieurw* 3(1), 42-50.
- Ahmad, S., N. Arifin, R. Nazar and I. Pop (2008). Free convection boundary layer flow over cylinders of elliptic cross section with constant surface heat flux. *European Journal of Scientific Research* 23, 613-625.
- Atmane, M., V. Chan and D. Murray (2003). Natural convection around a horizontal heated cylinder: the effects of vertical confinement. *Int. J. Heat Mass Transfer* 46, 3661-3672.
- Ayani, M., J. Esfahani, H. Niazmand and A. Sousa (2005). Transient laminar convection induced by a line heat source: a numerical study with primitive variables. *Scientia Iranica* 12, 247-254.
- Brodowicz, K. and W. Kierkus (1966). Experimental investigation of laminar free convection flow in air above horizontal wire with constant heat flux. *Int. J. Heat Mass Transfer* 9, 81-94.
- Cheng, C. (2006). Free convection heat and mass transfer from a horizontal cylinder of elliptic cross section in micropolar fluids. *International Communications in Heat and Mass Transfer* 33, 311-318.
- Grafsrnnigen, S. and A. Jensen (2012). Simultaneous PIV/LIF measurements of a transitional buoyant plume above a horizontal cylinder. *Int. J. Heat Mass Transfer* 55, 4195-4206.
- Grafsrnnigen, S., A. Jensen, B. Anders and B. PetterssonReif (2011). PIV investigation of buoyant plume from natural convection heat transfer above a horizontal heated cylinder. *Int. J. Heat Mass Transfer* 54, 4975-4987.
- Kitamura, K., F. Kami-Iwa and T. Misumi (1999). Heat transfer and fluid flow of natural convection around large horizontal cylinders. *Int. J. Heat Mass Transfer* 42, 4093-4106.
- Koizumi, H. and I. Hosokawa (1996). Chaotic behavior and heat transfer performance of the natural convection around a hot horizontal cylinder affected by a flat ceiling. *Int. J. Heat Mass Transfer* 39(5), 1081-1091.
- Kuehner, J., A. Hamed and J. Mitchell (2015). Experimental investigation of the free convection velocity boundary layer and plume formation region for a heated horizontal cylinder. *Int. J. Heat and Mass Transfer* 82, 78-97.
- Kuehner, J., J. Pflug, F. Tessier, A. Hamed, J. Franco and M. Marin (2012). Velocity measurements in the free convection flow above a heated horizontal cylinder. *Int. J. Heat Mass Transfer* 55, 4711-4723.
- Kumar-De, A. and A. Dalal (2006). A numerical study of natural convection around a square, horizontal, heated cylinder placed in an enclosure. *Int. J. Heat Mass Transfer* 49, 4608-4623.
- Miyabe, k. and T. Katsuhara (1972). Experimental investigation of the swaying plume above a heated horizontal cylinder. *Memoirs Kyushu Ins. Tech. Eng.* 2, 9-22.
- Morgan, V. (1975). The overall convective heat transfer from smooth circular cylinders. *Adv. Heat Transfer* 11, 199-264.
- Nakamura, H. and Y. Asako (1978). Laminar free convection from a horizontal cylinder with uniform cross section of arbitrary shape. *Bulletin of JSME* 21, 471-478.
- Nusselt, W. (1915). Das Grundgesetz des Wärmeüberganges. *Gesundheits-Ingenieur* 38, 477-482, 490-496.
- Sakr-Ramadan, Y., S. Berbish-Nabil, A. Abd-Aziz-Ali and S. Hanafi-Abdalla (2008). Experimental and numerical investigation of natural convection heat transfer in horizontal elliptic annuli. *J. Applied Sciences Research* 4(2), 138-155.